

# Vehicle Image Generation Going Well with the Surroundings

Jeesoo Kim<sup>1,\*</sup>, Jangho Kim<sup>1,\*</sup>, Jaeyoung Yoo<sup>1</sup>, Daesik Kim<sup>1,2</sup>, Nojun Kwak<sup>1</sup>  
<sup>1</sup>Seoul National University, <sup>2</sup>V.DO Inc.  
 {kimjiss0305|kjh91|yoojy31|nojunk@snu.ac.kr}  
 {daesik.kim@vdotdo.com}

## Abstract

Since the generative neural networks have made a breakthrough in the image generation problem, lots of researches on their applications have been studied such as image restoration, style transfer and image completion. However, there has been few research generating objects in uncontrolled real-world environments. In this paper, we propose a novel approach for vehicle image generation in real-world scenes. Using a subnetwork based on a precedent work of image completion, our model makes the shape of an object. Details of objects are trained by an additional colorization and refinement subnetwork, resulting in a better quality of generated objects. Unlike many other works, our method does not require any segmentation layout but still makes a plausible vehicle in the image. We evaluate our method by using images from Berkeley Deep Drive (BDD) and Cityscape datasets, which are widely used for object detection and image segmentation problems. The adequacy of the generated images by the proposed method has also been evaluated using a widely utilized object detection algorithm and the FID score. <sup>1</sup>

## 1. Introduction

Imagination has been regarded as a human’s exclusive ability for a long time. However, with the tremendous advance in deep neural networks, generative models have given a glimpse that machines can mimic some high level abilities of human beings such as imagination through generating plausible images. Quite a number of variants of autoencoders and generative adversarial networks have been introduced showing remarkable results even with natural images [3, 27, 17].

In spite of the advance of object generation models [29, 2, 11, 1], most of the generative models implicitly assume some rules when learning a domain. First, images used for training must be located in a consistent area and



Figure 1: The image on the left is the source image with a box given by hand and the image on the right is the result of our method. Unlike image inpainting, our method generates a vehicle inside the box. In addition to generating a vehicle with a reasonable orientation, our method naturally portrays the forest and the road surface around the vehicle.

usually placed in similar poses. For example, all digits are placed in the center of images in *MNIST* dataset [21] which is a hand-written digit dataset and frequently used to present the functionality of generative models. Likewise, many researches exploited the *Celeb* data [25] by cropping the faces of celebrities and aligning the locations of fiducial points such as eyes, nose and mouth to the same points. In this setting, the network would only learn to create segments in the locations where they usually exist, which is relatively easier than generating images in an arbitrary location and pose with various backgrounds. Also, images of the datasets mentioned above have clear visibility without any obstacles while many sights in the real world contain occlusions.

To compose an image and arrange objects in a non-trivial location, some researches have used the semantic layout to transform it into an image of a real scene. One of the frequently used datasets in this task is the *Cityscape* [5] which includes road scene images with pixel-wise annotations. Many researches have made a remarkable progress and succeeded to generate a realistic synthetic image using a semantic layout [19, 4, 31]. Hong et al. [15] has proposed a method that can generate an object in an arbitrary location assigned by a user using a semantic layout. Considering that the object detection task has been widely used for the autonomous driving, generating vehicles in images can be used as a practical data augmentation method for object de-

<sup>1</sup>\*Jeesoo Kim and Jangho Kim equally contributed to this work.

tectors which search for the bounding boxes of the objects. However, training a model and synthesizing an image using the semantic layout is an inefficient method since making a pixel-wise annotation requires a lot of time and human efforts. Demand for an inexpensive annotation in computer vision tasks is being raised steadily and one example of this is the weakly supervised object localization which tries to localize images only using image-level labels [36].

Meanwhile, image completion is a task of filling a missing area in an image. Several researches have shown that even unseen areas can be recovered using a properly trained model. The problem of these models is that an area having not enough clues is difficult to be reconstructed. They usually fail to complete some complicated texture such as the face of human or a portion of animals. Training these models with a single object category, they are capable of making the outline of the object but lack details of it. Since the appearance of the objects in image inpainting problems are not consistent like the images of *MNIST* or *Celeb*, image inpainting methods highly rely on the reconstruction loss rather than the adversarial loss which makes the object sharper. For this reason, the existing inpainting methods are very hard to generate a sharp image with an object inside.

In this paper, we propose a method to generate vehicles in given locations, which understands typical appearances of vehicles but with various orientations and colors. With a box given at an appropriate location with an appropriate size, our model can generate learned objects inside. The generated cars suit the surrounding background and even complete occluding objects ahead. Note that all we need to generate an object is just a box annotation while many other works in image translation [19, 4, 31, 15] require a segmented target map to transform it into a realistic image. To make a new object over an existing road image, users have to manually compose the segmentation layout. Our proposed method simply needs a rectangular-shaped mask to generate a vehicle, regardless of the location it is placed. Therefore, we utilize a dataset which contains box annotations around the objects in the images. Berkeley Deep Drive (BDD) dataset [32] is widely used for the tasks of object detection and image segmentation. By training the car areas annotated in the BDD dataset, we can generate a vehicle which goes well with its surroundings in an arbitrary location. The contributions of this paper are as the followings:

- We propose a method trying to generate a vehicle object in an image that goes well with the background.
- Unlike other methods using pixel-wise annotated information, only box annotations are used as a given knowledge.
- Our method is capable of generating vehicles over an empty road image as well as substituting the existing vehicles.

## 2. Related works

Experiencing tremendous advances in classification [13, 16], object detection [7, 24, 30, 20] and segmentation [26], computer vision has begun to make a progress in the field of generative models. Applications such as image restoration [9, 12, 33] and super-resolution [22, 6] have substantially benefited from the growth of generative models. In this part, we shortly review some of works related to our method.

In order to synthesize a lifelike image, many researches utilized label maps or contours as a guide to generate a real image. Isola et al. [19] proposed a method to transform any kind of blueprint into the desired output using GAN: for example, a sketch into a colored image, a gray-scale map into a satellite picture and a label map into a real city scape. Chen et al. [4] adopted a feature learning method by defining layer-wise losses. This enabled to transform a high resolution semantic layout into an actual image. Patch-based methods such as [31] enabled high quality image translation with an image size more than  $512 \times 512$ . Generating objects in locations decided by a user has been possible in the work of Hong et al. [15] using generative adversarial network. However, input layouts used in all of these methods are expensive to prepare in real world since it should be annotated pixel-wise. Despite the rich information they contain, making segmentation labels costs much more than just annotating bounding boxes.

Researches trying to generate more complicated context using clues in the image have been proposed recently. Image completion is a task of filling an appropriate image segment into a vacated region of a real world image. The model must learn to paint the image through the blank area. For example, in an image of a building, the corner of a window is removed and then the model must fill it up with glass and bricks aside. Coming to an image of a human face, one of the eyes or the nose is erased and the network recovers it in a natural form.

The Context Encoder (CE), an early work of image completion using a neural network [28], has been proposed for this problem. Using a channel-wise fully-connected layer between an encoder and a decoder, CE roughly generates pixels in the image using the encoder features. The work of [18] has approached this problem using dilated convolutions and a specific type of discriminator. The dilated convolution acts just the same as the original convolution except that the filter is applied to the feature skipping a few pixels or more. This derives the expansion of the receptive field without loss of resolution. Although both approaches can recover the missing parts of an image, it is impossible to generate a whole object. Even if trained only with a particular object, the result still suffers from a poor performance. This is because the model bumbles among many choices of how the object will be generated. Since the completion model can predict the shape and surrounding context roughly, we use

it as a primary module of our method.

### 3. Approach

In this paper, we assume that every object can be expressed using two traits, shape and texture. Our method consists of two consecutive networks learning each of these properties.

#### 3.1. ShapeNet

As we assume that the segmentation layout is not given, we adopt an image completion model which understands the surrounding texture around the erased area. The architecture used in our ShapeNet (Snet) is the same as that of [18]. Generally, most generative models downsample the input into a vector and reconstruct it back to the scale of the original input. However, for the image completion task, the information from the features nearby is more important. Therefore, decreasing the resolution only to a half is adequate to fill the blank area. We adopted this philosophy and applied it to the Snet. Also, to extend the receptive field of the features in each layer, dilated convolution [34] is used in the middle of the network. In this way, the network can reflect the information not only from the pixels adjacent to the blank area but also from those far away. This highly encourages the network to decide how the object should be placed and how the occluding object should be completed. Strided convolutions are used for downsampling instead of pooling layers. At the end of the Snet, the network reconstructs the gray-scaled image of the original input so that the model concentrates on constructing the pose and shape of the generated object, not the color or details of the context. The detailed procedure of Snet can be summarized as follows:

$$\hat{I}_{gray} = S([I'; M]). \quad (1)$$

Here,  $I'$  represents the image of which an area corresponding to the mask  $M$  has been removed and  $S(\cdot)$  denotes the Snet. Note that the mask  $M$  is not a segmentation layout but a rectangular binary map which corresponds to the bounding box of the object. The encoding step includes 3 steps of downsampling and 4 types of dilated convolution (rate = 1, 2, 4, 8). The decoding step upsamples the features into the original scale using bilinear interpolations and convolution layers. Pixels outside the generated region is preserved as we do not wish any change outside of the box.

After the Snet generates an image, only the region inside the box is combined with the stored background pixels. By doing this, only the change occurred inside of the box is taken into consideration. The Snet is trained to minimize the  $L_1$  distance between the synthesized gray-scale image  $\hat{I}_{gray}$  and the original gray scale image  $I_{gray}$  as in (2).

$$L_S = \|I_{gray} - \hat{I}_{gray}\|_1. \quad (2)$$

#### 3.2. TextureNet

Complicated visual properties of real objects often disrupt the learning of generative models. When it comes to generating a car, details such as headlights, taillights or the windshield of a car may vary a lot. If the Snet makes a rough sketch, the TextureNet (Tnet) adds details by painting colors on the sketched gray scale image. We have adopted the architecture in [35] which was used for a colorization task. The Tnet can be summarized as follows:

$$\hat{I}_{color} = T_{color}(I_{gray}^p, I') \quad (3)$$

$$\hat{I} = T_{refine}(\hat{I}_{color}) \quad (4)$$

$$L_T = CrossEntropy(I, \hat{I}_{color}) + \lambda \|I - \hat{I}\|_1. \quad (5)$$

Tnet is divided into two components:  $T_{color}(\cdot)$  which paints colors on the gray patch image  $\hat{I}_{gray}^p$  and paste it back to the masked image  $I'$ , and  $T_{refine}(\cdot)$  which corrects the details of the colorized image  $\hat{I}_{color}$  as in (3) and (4), respectively. After the  $T_{color}$  classifies the color classes of all pixels, the colorized image of  $\hat{I}_{gray}$  is pasted back to  $I$ , which produces  $\hat{I}_{color}$ .

We crop the patch image  $I_{gray}^p = Crop(I_{gray}, M)$  where the object is to be generated since the remaining region does not need any colorization nor manipulation. In the Tnet,  $T_{color}$  in (3) learns the color distribution of cars in detail. As in [35],  $T_{color}$  predicts the values of each pixel in the CIELab color space. Since the gray scale image corresponds to the lightness, the model should predict the remaining a and b values. A pretrained VGG-19 network is used to extract features from the gray image. After that, a  $1 \times 1$  convolution filter outputs a tensor with the depth of 313. Dividing the ab color space into 313 bins, the  $T_{color}$  turns the colorization problem into a classification problem which is much more easier than directly generating images having various occlusions and a wide color variation. Each channel of the last convolutional feature corresponds to the score of each color bin and one of the colors is chosen in every pixels by the softmax operator. The cost is calculated by the cross-entropy function between the output and the Lab-encoded ground-truth values as in the first term of (5). The color is painted solely on the patch image, which can be awkward when the patch is pasted back to the original image. Therefore, we use an additional network module  $T_{refine}$  that encourages the object to get along with the surroundings of the image. Using the same structure with the Snet, this module highly sharpen the blurry results of colorized images and adaptively optimize the colors of the neighboring objects such as occluding cars, road segments or parts of buildings. This module is trained adversarially using a global-local discriminator along with a small reconstruction L1-loss as shown by the second term in (5).

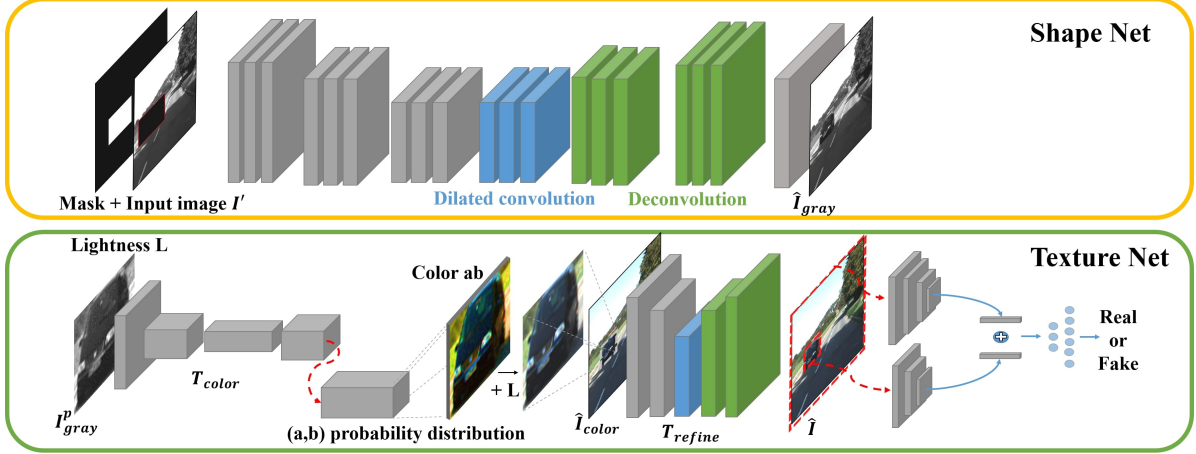


Figure 2: Overall architecture. The top-side of the figure shows the Snet and the bottom-side shows the Tnet which is composed of  $T_{color}$  and  $T_{refine}$ . Bilinear interpolation is used to recover the resolution of  $\hat{I}_{color}$ .

### 3.3. Global-Local discriminator

A global-local context discriminator is used to train our model in the same way as in [18]. The overall discriminator  $D$  consists of one global discriminator  $D_{global}$  and one local discriminator  $D_{local}$ . The global discriminator takes the entire image  $I$  (real) or  $\hat{I}$  (generated) as an input and the local discriminator takes the patch image  $I_p$  or  $\hat{I}_p$  inside the annotated box from the respective image  $I$  or  $\hat{I}$ . The size of the patch image is normalized to  $64 \times 64$  by ROI-pooling. Each discriminator is followed by a fully connected layer. After that, both features are concatenated into a single vector and then processed by a single fully connected layer. A sigmoid output produces an outcome which is trained to correctly decide whether the given image is real or completed by the model. This encourages the model to depict sophisticated details of the object. The discriminator  $D$  and  $T_{refine}$  are trained in an adversarial way as follows:

$$\begin{aligned} \min_{T_{refine}} \max_D \mathbb{E}_{I_p, I \sim P_{data}} [\log(D(I_p, I))] \\ + \mathbb{E}_{\hat{I}_{color} \sim P_{T_{color}(\hat{I}_{gray})}} [1 - \log(D(\hat{I}_p, \hat{I}))] \end{aligned} \quad (6)$$

We may consider the colorized image input  $\hat{I}_{color}$  from the  $T_{color}$  as a noise. This allows our model to be trained adversarially.

### 3.4. Overall training

Unlike the training of image translation models [15], our method only needs the region where objects lie on. As only one vehicle is given as a target, the model completes one vacated region at a time. Therefore, the actual amount of training data equals to the number of images times the average number of vehicles in one image.

To enhance the quality of the results, Snet and  $T_{color}$

are pre-trained individually beforehand. We take the box-annotated patch away from the gray-scaled image  $I_{gray}$  and feed it to the Snet as an input  $I'$  with a mask  $M$  which helps the model find the area of interest. The Snet is trained to minimize  $L_S$ , the  $L_1$  distance loss between the output of Snet and the ground truth gray scale image  $I_{gray}$ , as in (2). The patch image from the real sample  $I_{gray}^p$  is given to the  $T_{color}$ .  $T_{color}$  is trained to minimize the cross-entropy loss mentioned in Section 3.2.

After the pre-training, all components are connected to form a single pipeline and jointly optimized. Instead of  $I_p'$ ,  $T_{color}$  receives the patch image of the generated gray-scaled image  $\hat{I}_{gray}$ . A differentiable operation converts  $\hat{I}_{gray}$  into the lightness channel of Lab color space before the forwarding of  $T_{color}$ . The resulting colorized patch image  $\hat{I}_{color}$  is pasted back to the groundtruth image  $I$  by an affine transformation. Then the  $T_{refine}$  tries to reconstruct the full-scale image. To train the discriminator, the original image  $I$  and the generated image  $\hat{I}$  are given to  $D$  which discriminates them as real and fake, respectively.  $D$  is updated solely and then  $T_{refine}$  is updated to deceive  $D$  so that it classifies  $\hat{I}$  as a real sample. The whole model can be trained simultaneously with all losses altogether. However, we have found that training each module respectively shows better results.

## 4. Experiments

### 4.1. Dataset

Among various objects, we have chosen to specifically concentrate on the car which has more clear visibility compared to other objects in the data. Its shape is physically monotonous but differs according to the perspective. Also, as most cars usually run observing the traffic law, it is quite predictable for a human to imagine a car on the road. There-



Figure 3: Results from our method and the baseline [18]. From top to bottom, 1) completed gray-scaled results of Snet, 2) results colorized by  $T_{color}$ , 3) final results of Tnet after refinement, and 4, 5) results of the baselines. Compared to the results of the baselines, our model depicts the details better since the refine module of Tnet can produce elaborate outputs. To present how well our method performs by itself, no post-processing is applied to all results.

fore, the task of generating cars on the scene is reasonable but not a trivial task since it requires lots of contextual variables.

BDD100K is a dataset including videos filmed by running cars [32]. The BDD challenge dataset, which we use in this paper, contains 70,000 training images with an average of 9.7 cars per image and 10,000 validation samples. Images are captured from 100K driving videos covering various regions of USA. After resizing the the resolution to  $320 \times 180$  for the stable training, boxes sized under 10 pixels either horizontally or vertically are excluded in the training since they are so small that it is hard to acknowledge them as cars, which makes it meaningless to generate them. Also, a large vacated area is known to be hard to fill by the image completion frameworks. Therefore, we exclude boxes bigger than  $64 \times 50$  since both the baseline and our method show poor results on them. Some failure cases with a large box are shown in Fig. 7.

## 4.2. Vehicle generation subject to the surroundings

We evaluated our trained model by generating vehicles on test images of BDD100K dataset. Since there is no other

research generating an object in a given position only using the box annotation, we set the researches of [18] and [23] used in the image completion problem as the baseline models. As the image completion problem that the baseline model tries to solve is quite similar to our problem, the baseline holds the capacity to generate objects if trained properly. Instead of vacating a random region of the image as in [18], we only deleted the region where a vehicle exists and regenerated a new vehicle. As the baseline models only witness particular appearances, this makes them possible to generate an object, though they fail to express the details of objects as explained in this paper.

Some results of [18] are shown in the fourth row of Fig. 3. Cars generated at the center of the images mostly show their backside since most of the cars are running forward. For the boxes located between the road and the sidewalk, the cars are generated slightly askew as the camera usually shoots them in the diagonal direction. The overall appearances of all results resemble the real vehicles but the details such as taillights and wheels lack delicacy. Despite using the global-local discriminator described in Section 3.3, the baseline model generates blurry results. An ex-

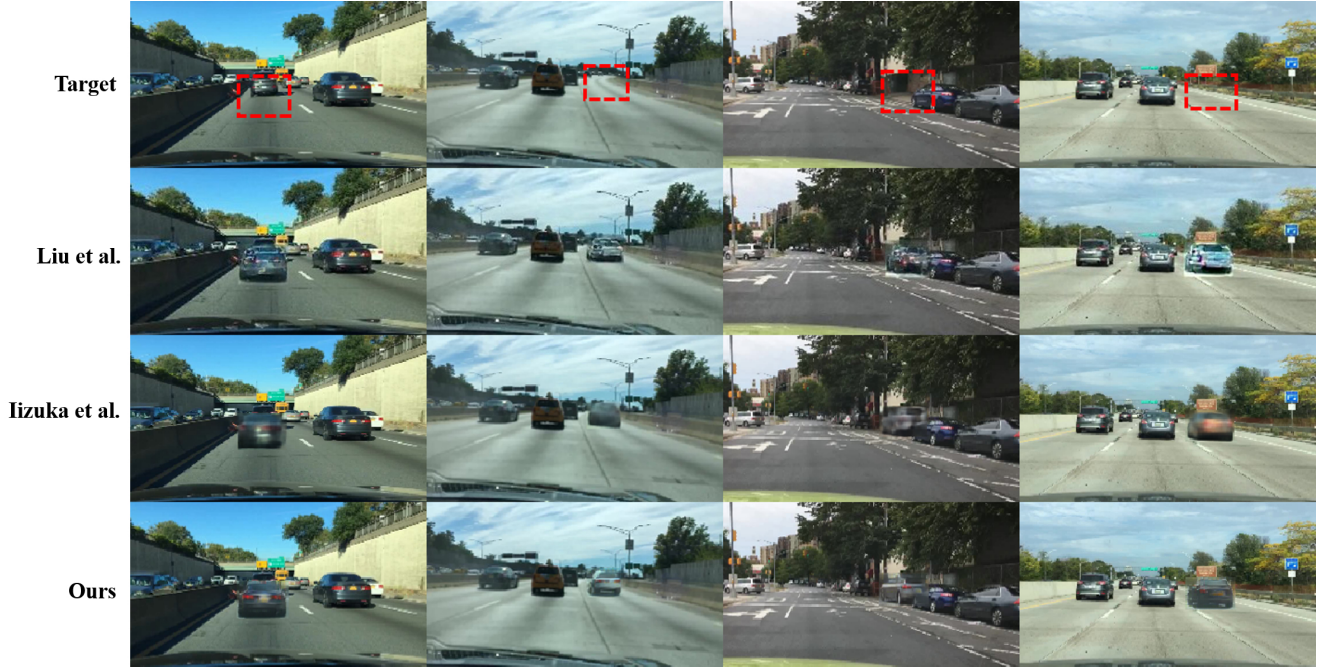


Figure 4: Generating vehicles on empty roads. Target regions where the vehicles are to be generated are marked by red rectangles in the first row. With proper boxes given, both the baselines and our method draw vehicles inside.



Figure 5: Our results generated over the *Cityscape* dataset. The red arrows indicate where the vehicles are generated.

cessive abuse of adversarial loss easily corrupts the model and impedes the training, which is why we mitigated the problem by our method. Results from the work of [23], the last row in Fig. 3, are considerably poor compared to other methods. Using the perceptual loss introduced by Gatys *et al.* [10], the model produces a reasonable background segments and makes an appropriate outline of a vehicle. However, the texture inside is quite noisy, which seems to draw cars inside a car, and hard to be perceived as a car. The third row of Fig. 3 shows some results of our method. In our method, the outline of vehicles are clearly visible and parts such as the taillights and wheels are described delicately. Also, the texture around the generated car suits the surrounding background. The paved roads are naturally connected at the bottom side. Furthermore, the model can recognize a building or a bush behind and can reflect it in the background.

Although not presented in this paper, we also have tried to use the refine network module ( $T_{refine}$ ) directly after the

Snet producing colored images instead of black and white images. However, the adversarial loss easily corrupts the model making the images unrecognizable. In Fig.3, the results of Snet (the first row) and Iizuka *et al.* (the fourth row) are similarly blurry and incomplete. Adding clues of texture by colorization (the second row) highly helps the training of  $T_{refine}$  in which the adversarial loss is dominant. Also, while  $T_{color}$  focuses on painting the vehicle regardless of its surroundings,  $T_{refine}$  makes up for the inconsistent surroundings.

### 4.3. Vehicle generation on an empty road

After training the model, we experimented the situation in which our model generates cars at given locations where no car existed in the original images, which is the eventual objective of this paper. While training, we feed our model with car images containing an empty box at the object location as shown in Fig. 2. Therefore, if the model has properly learned how to complete a blank box, generating a car upon

Table 1: Object detection score (recall in %) when Tnet is additionally used (Ours) or not (Baseline). Single Shot multibox Detector(SSD) [24] is used to evaluate how well the objects are generated. Weights of SSD are pre-trained using PascalVOC dataset. We only report the recall score at the target region since vehicles outside are not under consideration.

Method	Confidence threshold	
	0.12	0.3
Original BDD	87.42	78.59
Baseline[18]	63.35	50.23
<b>Ours</b>	<b>73.12</b>	<b>60.24</b>



Figure 6: Detection results of generated objects. Boxes in purple shows the detection result of SSD. The top row shows the generated sample that our method succeeded to deceive the detector to perceive it as a vehicle while the baseline failed and the second row shows the case where both methods deceived the detector in spite of the poor quality of the baseline. In spite of our far better quality, SSD occasionally detects the deformed results of the baseline as a car.

an empty road is possible since it shares the same procedure with substituting an object. Images of the road with no cars on it are chosen, which would have been never used in training since it has no annotation box on it. Fig. 4 shows the results how well our method generates objects on empty roads where we asked it to. Given a reasonable location, the model is capable of generating a car with a random context. Especially, our method shows a remarkable performance when it comes to generating a car parking alongside the road. Even if there is a car occluding the target vehicle, the model also completes the occluding one as well.

#### 4.4. Vehicle generation on Cityscape dataset

To show that our method is not restricted to the dataset it is trained on, we apply our network trained by BDD to generate cars on images from the *Cityscape* dataset [5]. Since, both of the datasets contain road scene images in the view of the drivers, the perspective and overall aspects are quite similar except that BDD is taken in U.S.A and *Cityscape* in Germany. Fig. 5 shows the results of our model applied to the *Cityscape* dataset. Without the red arrow indicating the generated vehicle, it is difficult to recognize which one is the generated vehicle at one glance.

#### 4.5. Effectiveness of using Texture net

Bringing the global-local discriminator to the end of Snet and changing the output dimension to RGB channels is equivalent to the work of [18]. Though we have shown the qualitative improvement in the figures above, we report an additional numerical comparison to prove the effectiveness of Tnet. We apply the Single Shot multibox Detector (SSD) [24], a widely used object detection algorithm, to the images generated by our method and the baseline[18]. Vehicles from the original images are substituted by both methods. If objects are generated properly, the detector should be able to locate them in the image.

Our model and the baseline [18] have been trained using the training data in BDD100K and the evaluation has been carried out with the validation data. Since only the object to be generated is under consideration, vehicles detected outside the generated region are ignored. In other words, we only evaluate the recall of SSD, which is the ratio whether the detector finds the generated object or not. In the dataset, there are a total of 6,020 vehicles to recall that satisfy our size constraints. Since the detector is trained using PascalVOC dataset [8], it is fair enough to compare the baseline and our method applied to BDD100K dataset.

Table 1 shows the recall scores of SSD on BDD dataset. For the original BDD images, SSD detects vehicles in the box area at a rate of 78.59% using the confidence threshold of 0.3 and 87.42% using the confidence threshold of 0.12 as shown in Table 1. In both class confidence score thresholds, our method highly precedes the baseline by about 10% points. Additionally, we analyze the detection result of which the threshold is 0.12. Samples, which our method successfully makes the detector perceive as vehicles while the baseline fails to, occupy 17.24% while the opposite case records 7.47%. Our method has substantially more number of vehicles with superiority. One example of this case is shown in the top row of Fig. 6. Meanwhile, though both methods successfully deceive the detector in many cases, quite a lot of samples generated by the baseline suffer from a qualitatively poor performance. This case is presented in the bottom row of Fig. 6.



Figure 7: Failure cases. On the first row lie some single channel outputs of Snet and on the second row lie the corresponding 3-channel outputs of Tnet. Once the result from Snet is distorted, the Tnet fails to complete the image. From the left to the right, we show failure cases of boxes having abnormal aspect ratio, unsuccessful front side expression due to the data imbalance, being disturbed by the illumination and excessively wide boxes.

Table 2: The FID scores of the methods used in this paper. Only the generated region is used for the evaluation since the rest of the area is not synthesized.

Method	FID score
Iizuka <i>et al.</i> [18]	112.3
Liu <i>et al.</i> [23]	50.54
<b>Ours</b>	41.04

#### 4.6. Measuring generation quality

Frechet inception distance (FID) score [14] is a measure frequently used to evaluate the generation quality of generative models. Using a pre-trained Inception-V3, FID compares the statistics of generated images to the real ones. Generally, a low FID score implies that the generated samples have similar activation distributions to those of the real samples. A blurry and noisy result usually increases the FID score. Also, uni-modal result, which is generally referred as *mode collapse*, is known to increase the FID score as well.

In Table 2, we assess the quality of images generated by each method. Images from [18] roughly have the appearance of vehicles but record the worst FID score. This attributes to the abstractly depicted context of each vehicle. The work of Liu *et al.* shows an intermediate level of FID score. Though the silhouette of the generated sample resembles the vehicle, the texture inside is rather a noise which causes an increase in the FID score. Our method has the lowest FID score, which means that our method generates samples that have the most similar distribution to that of real samples.

### 5. Discussion

The object detection dataset includes annotations indicating the location where the car exists, not where the car may be. This enforces us to give the model a box at a reasonable position manually. Although the most important merit of our method is that we only use a box annotation to

generate a vehicle, the necessity of giving a box candidate still remains. With a highly predictive scene understanding model that can suggest the location where the vehicle may be, we expect a fully-automated vehicle image augmentation would be possible. In the supplementary, we show a preliminary result showing a hint towards this end.

Also, wide boxes, which correspond to the cars near the camera, usually fail to be filled, which is the drawback of the image completion models. Some of the failure examples are given in Fig. 7.

The total amount of training data is relatively small compared to any other works using generative models. We attribute the blurry effect and insufficient representation embedding to the lack of the training data. Furthermore, objects with different locations and colors suffer from a severe data imbalance. We expect that our method would go well with a large-sized and well balanced image dataset.

### 6. Conclusion

We tackled a problem to generate vehicles at designated locations over images of real scenes. To solve this problem, we used an architecture composed of two subnetworks which generate the shape and the texture of the vehicle respectively. The Snet roughly completes the shape of the car according to the surroundings while the Tnet decides the details of the generated vehicle resulting in a better generating performance. Consequently, our method can generate objects going well with the surroundings in arbitrary locations. This is highly expected to be a foundation research for image augmentation researches. Though we have proposed a preliminary method in the supplementary material proposing the region where the object is to be generated, the problem of giving a sophisticated location still remains. Adding a fully automated reasoning process that can designate the location on which an object would be plausible, our method can be used as a practical data augmentation system and we leave this for our future work.

## References

- [1] M. Arjovsky, S. Chintala, and L. Bottou. Wasserstein gan. *arXiv preprint arXiv:1701.07875*, 2017. **1**
- [2] D. Berthelot, T. Schumm, and L. Metz. Began: boundary equilibrium generative adversarial networks. *arXiv preprint arXiv:1703.10717*, 2017. **1**
- [3] A. Brock, J. Donahue, and K. Simonyan. Large scale gan training for high fidelity natural image synthesis. *arXiv preprint arXiv:1809.11096*, 2018. **1**
- [4] Q. Chen and V. Koltun. Photographic image synthesis with cascaded refinement networks. In *The IEEE International Conference on Computer Vision (ICCV)*, volume 1, 2017. **1, 2**
- [5] M. Cordts, M. Omran, S. Ramos, T. Rehfeld, M. Enzweiler, R. Benenson, U. Franke, S. Roth, and B. Schiele. The cityscapes dataset for semantic urban scene understanding. In *Proceedings of the IEEE conference on computer vision and pattern recognition*, pages 3213–3223, 2016. **1, 7**
- [6] R. Dahl, M. Norouzi, and J. Shlens. Pixel recursive super resolution. *arXiv preprint arXiv:1702.00783*, 2017. **2**
- [7] J. Dai, Y. Li, K. He, and J. Sun. R-fcn: Object detection via region-based fully convolutional networks. In *Advances in neural information processing systems*, pages 379–387, 2016. **2**
- [8] M. Everingham, L. Van Gool, C. K. Williams, J. Winn, and A. Zisserman. The pascal visual object classes (voc) challenge. *International journal of computer vision*, 88(2):303–338, 2010. **7**
- [9] L. Galteri, L. Seidenari, M. Bertini, and A. Del Bimbo. Deep generative adversarial compression artifact removal. **2**
- [10] L. A. Gatys, A. S. Ecker, and M. Bethge. A neural algorithm of artistic style. *arXiv preprint arXiv:1508.06576*, 2015. **6**
- [11] I. Gulrajani, F. Ahmed, M. Arjovsky, V. Dumoulin, and A. C. Courville. Improved training of wasserstein gans. In *Advances in Neural Information Processing Systems*, pages 5767–5777, 2017. **1**
- [12] J. Guo and H. Chao. One-to-many network for visually pleasing compression artifacts reduction. **2**
- [13] K. He, X. Zhang, S. Ren, and J. Sun. Deep residual learning for image recognition. In *Proceedings of the IEEE conference on computer vision and pattern recognition*, pages 770–778, 2016. **2**
- [14] M. Heusel, H. Ramsauer, T. Unterthiner, B. Nessler, and S. Hochreiter. Gans trained by a two time-scale update rule converge to a local nash equilibrium. In *Advances in Neural Information Processing Systems*, pages 6626–6637, 2017. **8**
- [15] S. Hong, X. Yan, T. Huang, and H. Lee. Learning hierarchical semantic image manipulation through structured representations. *arXiv preprint arXiv:1808.07535*, 2018. **1, 2, 4**
- [16] J. Hu, L. Shen, and G. Sun. Squeeze-and-excitation networks. *arXiv preprint arXiv:1709.01507*, 2017. **2**
- [17] H. Huang, R. He, Z. Sun, T. Tan, et al. Introvae: Introspective variational autoencoders for photographic image synthesis. In *Advances in Neural Information Processing Systems*, pages 52–63, 2018. **1**
- [18] S. Iizuka, E. Simo-Serra, and H. Ishikawa. Globally and locally consistent image completion. *ACM Transactions on Graphics (TOG)*, 36(4):107, 2017. **2, 3, 4, 5, 7, 8**
- [19] P. Isola, J.-Y. Zhu, T. Zhou, and A. A. Efros. Image-to-image translation with conditional adversarial networks. *arXiv preprint*, 2017. **1, 2**
- [20] J. Jeong, H. Park, and N. Kwak. Enhancement of ssd by concatenating feature maps for object detection. *arXiv preprint arXiv:1705.09587*, 2017. **2**
- [21] Y. LeCun, L. Bottou, Y. Bengio, and P. Haffner. Gradient-based learning applied to document recognition. *Proceedings of the IEEE*, 86(11):2278–2324, 1998. **1**
- [22] C. Ledig, L. Theis, F. Huszár, J. Caballero, A. Cunningham, A. Acosta, A. Aitken, A. Tejani, J. Totz, Z. Wang, et al. Photo-realistic single image super-resolution using a generative adversarial network. *arXiv preprint*, 2017. **2**
- [23] G. Liu, F. A. Reda, K. J. Shih, T.-C. Wang, A. Tao, and B. Catanzaro. Image inpainting for irregular holes using partial convolutions. In *Proceedings of the European Conference on Computer Vision (ECCV)*, pages 85–100, 2018. **5, 6, 8**
- [24] W. Liu, D. Anguelov, D. Erhan, C. Szegedy, S. Reed, C.-Y. Fu, and A. C. Berg. Ssd: Single shot multibox detector. In *European conference on computer vision*, pages 21–37. Springer, 2016. **2, 7**
- [25] Z. Liu, P. Luo, X. Wang, and X. Tang. Deep learning face attributes in the wild. In *Proceedings of the IEEE International Conference on Computer Vision*, pages 3730–3738, 2015. **1**
- [26] J. Long, E. Shelhamer, and T. Darrell. Fully convolutional networks for semantic segmentation. In *Proceedings of the IEEE conference on computer vision and pattern recognition*, pages 3431–3440, 2015. **2**
- [27] T. Miyato, T. Kataoka, M. Koyama, and Y. Yoshida. Spectral normalization for generative adversarial networks. *arXiv preprint arXiv:1802.05957*, 2018. **1**
- [28] D. Pathak, P. Krahenbuhl, J. Donahue, T. Darrell, and A. A. Efros. Context encoders: Feature learning by inpainting. In *Proceedings of the IEEE Conference on Computer Vision and Pattern Recognition*, pages 2536–2544, 2016. **2**
- [29] A. Radford, L. Metz, and S. Chintala. Unsupervised representation learning with deep convolutional generative adversarial networks. *arXiv preprint arXiv:1511.06434*, 2015. **1**
- [30] J. Redmon, S. Divvala, R. Girshick, and A. Farhadi. You only look once: Unified, real-time object detection. In *Proceedings of the IEEE conference on computer vision and pattern recognition*, pages 779–788, 2016. **2**
- [31] C. Wang, H. Zheng, Z. Yu, Z. Zheng, Z. Gu, and B. Zheng. Discriminative region proposal adversarial networks for high-quality image-to-image translation. *arXiv preprint arXiv:1711.09554*, 2017. **1, 2**
- [32] H. Xu, Y. Gao, F. Yu, and T. Darrell. End-to-end learning of driving models from large-scale video datasets. *arXiv preprint*, 2017. **2, 5**
- [33] J. Yoo, S.-h. Lee, and N. Kwak. Image restoration by estimating frequency distribution of local patches. In *Proceedings of the IEEE Conference on Computer Vision and Pattern Recognition*, pages 6684–6692, 2018. **2**

- [34] F. Yu and V. Koltun. Multi-scale context aggregation by dilated convolutions. *arXiv preprint arXiv:1511.07122*, 2015. [3](#)
- [35] R. Zhang, P. Isola, and A. A. Efros. Colorful image colorization. In *European Conference on Computer Vision*, pages 649–666. Springer, 2016. [3](#)
- [36] B. Zhou, A. Khosla, A. Lapedriza, A. Oliva, and A. Torralba. Learning deep features for discriminative localization. In *Proceedings of the IEEE conference on computer vision and pattern recognition*, pages 2921–2929, 2016. [2](#)

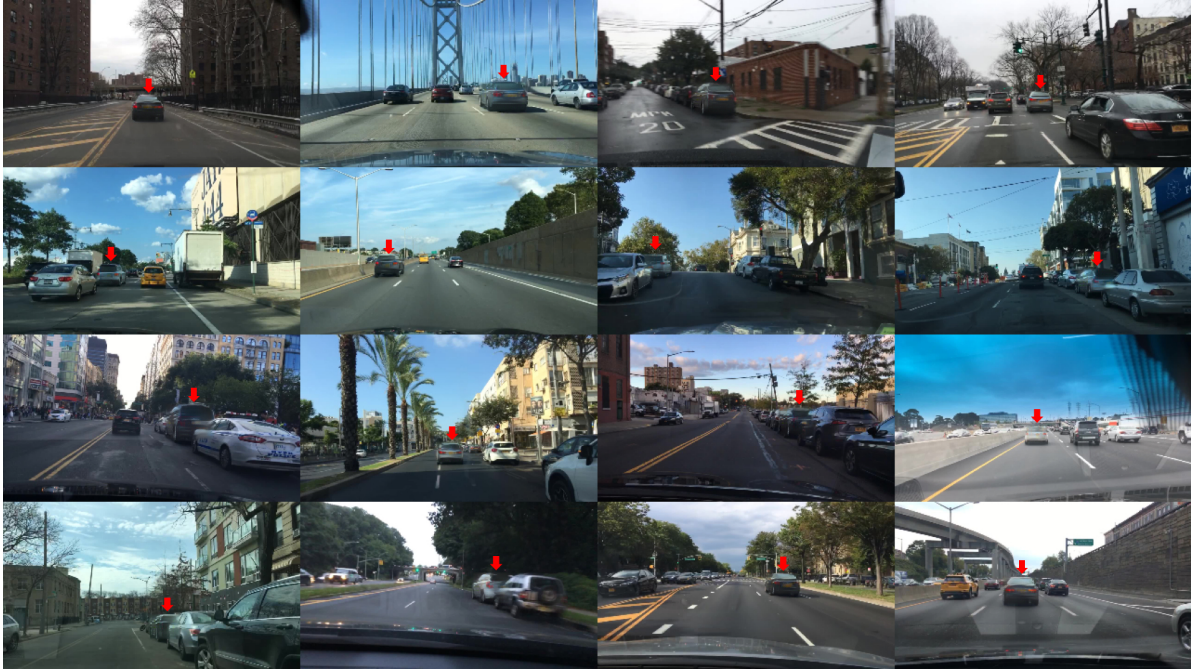


Figure 8: Replacing vehicles in the BDD 100K dataset with the results of our method. Generated cars are marked by red arrows. For a better quality, we additionally applied a post-processing with alpha blending around the boundary region of the box. Best viewed in color.

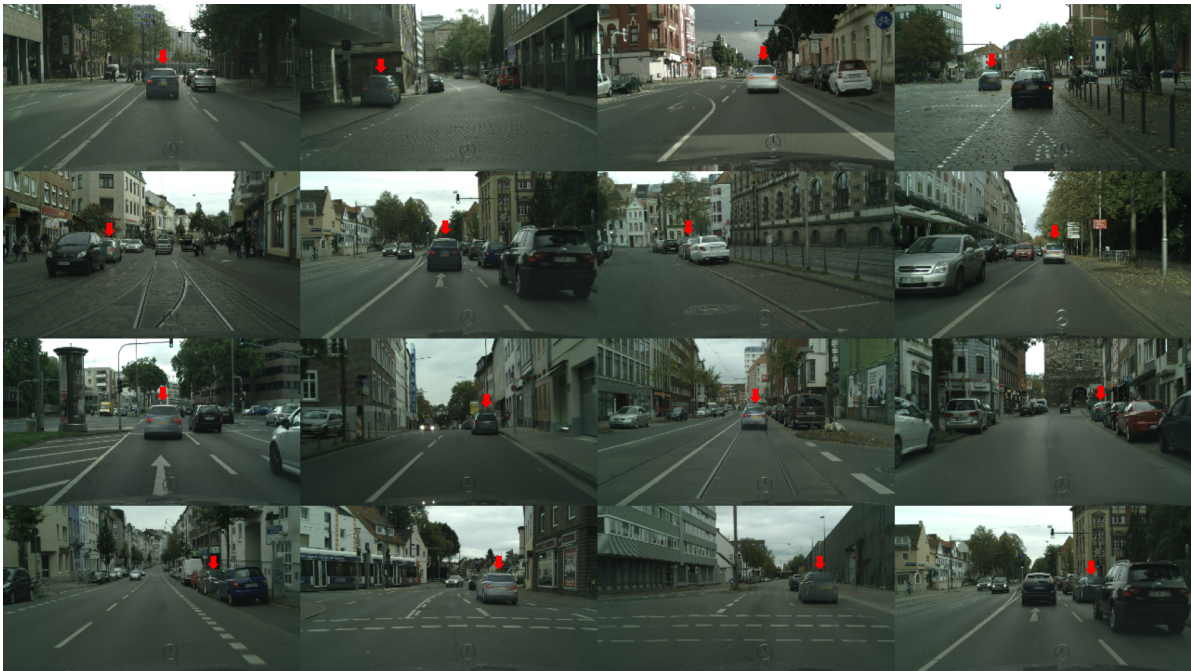


Figure 9: Replacing vehicles in the Cityscape dataset with the results of our method trained by the BDD 100K dataset. Generated cars are marked by red arrows. For a better quality, we additionally applied a post-processing with alpha blending around the boundary region of the box. Best viewed in color.

Table 3: The architecture of Snet. All layers are followed by a LeakyReLU function.

Snet				
Layer	out channel dim.	kernel size	stride	dilation
Conv2d	64	5	1	
Conv2d	128	3	2	
Conv2d	128	3	1	
Conv2d	256	3	2	
Conv2d	256	3	1	
Conv2d	256	3	1	
Conv2d	256	3	1	2
Conv2d	256	3	1	4
Conv2d	256	3	1	8
Conv2d	256	3	1	16
Conv2d	256	3	1	
Conv2d	256	3	1	
ConvTranspose2d	128	4	2	
Conv2d	128	3	1	
ConvTranspose2d	64	4	2	
Conv2d	64	3	1	
Conv2d	32	3	1	
Conv2d	1	3	1	
Sigmoid				

